Electron Transfer in Amino Acid·Nucleic Acid Base Complexes: EPR, ENDOR, and DFT Study of X-Irradiated *N*-Formylglycine·Cytosine Complex Crystals

Einar Sagstuen,*,† David M. Close,‡ Randi Vågane,† Eli O. Hole,† and William H. Nelson§

Department of Physics, University of Oslo, P.O. Box 1048 Blindern, N-0316 Oslo, Norway, Department of Physics, East Tennessee State University, Johnson City, Tennessee 37614, and Department of Physics and Astronomy, Georgia State University, Atlanta, Georgia 30303

Received: February 20, 2006; In Final Form: May 3, 2006

Single crystals of the 1:1 complex of the nucleic acid base cytosine and the dipeptide *N*-formylglycine (C·NFG) have been irradiated at 10 and 273 K to doses of about 70 kGy and studied at temperatures between 10 and 293 K using 24 GHz (K-band) and 9.5 GHz (X-band) electron paramagnetic resonance (EPR), electron nuclear double resonance (ENDOR), and ENDOR-induced EPR (EIE) spectroscopy. In this complex, the cytosine base is hydrogen bonded at positions N3 and N4 to the carboxylic group of the dipeptide, and the N3 position of cytosine has become protonated by the carboxylic group. At 10 K, two major radicals were characterized and identified. One of these (R1) is ascribed to the decarboxylated *N*-formylglycine one-electron oxidized species. The other (R2) is the N3-protonated cytosine one-electron reduced species. A third minority species (R3) appears to be a different conformation or protonation state of the one-electron reduced cytosine radical. Upon warming, the R2 and R3 radicals decay at about 100 K, and at 295 K, the only cytosine-centered radicals present are the C5 and C6 H-addition radicals (R5, R6). The R1 radical decays at about 150 K, and a glycine backbone radical (R4) grows in slowly. Thus, in the complex, a complete separation of initial oxidation and reduction events occurs, with oxidation localized at the dipeptide moiety, whereas reduction occurs at the nucleic acid base moiety. DFT calculations indicate that this separation is driven by large differences in electron affinities and ionization potentials between the two constituents of the complex. Once the initial oxidation and reduction products are trapped, no further electron transfer between the two constituents of the complex takes place.

1. Introduction

Considerable efforts have been made in the past decades to unravel the radiation damage processes occurring in DNA initiated by both the direct and indirect actions of ionizing radiation.[1−5] However, a full understanding of the in vivo radiation chemistry of DNA also requires an understanding of how the cellular environments of DNA modify those processes taking place in DNA itself. The most common environment is that of DNA tightly packaged in chromatin, although variations occur, for example, when DNA is being translated and transcribed.

As early as in 1961, Alexander et al.[6] demonstrated, using electron paramagnetic resonance (EPR) spectroscopy, that irradiation of nucleoproteins indicated energy transfer from the protein to DNA. Similar results were obtained by Lillicrap and Fielden[7] and Olast and Bertinchamps.[8] Quite conclusive evidence for electron transfer between the protein and DNA was obtained by Cullis et al.[9] These authors showed that electrons from the histones in chromatin transfer to DNA but that the holes do not transfer. This would result in an increase in the DNA anion radicals and would result in a loss of DNA cation radicals by recombinations. Faucitano et al.[10] interpreted their results similarly, concluding that excess capture of electrons by thymine and cytosine was key for the spin transfer mechanism.

Weiland and Hüttermann[11] published a very detailed study of electron transfer from histone to DNA in chromatin. The yield of DNA radicals in chromatin at low temperature was found to be about two times that found for DNA alone, which was considered strong evidence for electron transfer from histone to DNA in accord with earlier results of Faucitano et al.[10] and Cullis et al.[9] In particular, the ratio of anion to cation radicals in the DNA component of chromatin was found to be approximately two times that in DNA alone. This large relative loss of DNA cations, or gain in anions, was attributed to an increase in the concentration of one-electron-reduced radical components stabilized in DNA or, equivalently, to hole transfer from DNA to the histone.

If it is the oxidation pathway that leads to strand breaks, then these results suggest that the histones, by providing electrons that can combine with radicals in the oxidative cohort of DNA, provide a radioprotective effect to DNA.[5] However, warming chromatin, irradiated at 77, to 300 K largely reduces the total radical concentration without significant changes in the DNA/protein radical ratio. Apparently, electrons and/or holes are thermally mobilized in both components without any exchange between the components. If the stable end products reflect a doubling in reductive damage while oxidative damage remains the same, an increase in frequency and complexity of clustered

* To whom correspondence should be addressed. Tel.:+47 228 55653. Fax:+47 228 55671. E-mail: einar.sagstuen@fys.uio.no.
† University of Oslo.
‡ East Tennessee State University.
§ Georgia State University.

10.1021/jp0610822 CCC: $33.50
Published on Web 06/17/2006

SCHEME 1. Cytosine·*N*-formylglycine (C·NFG)

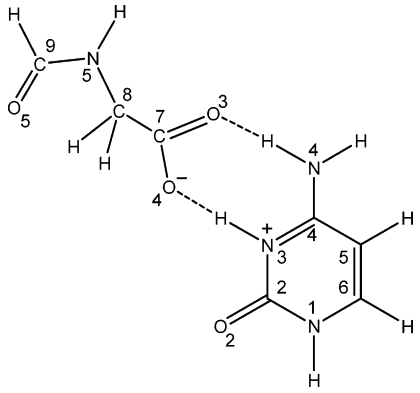

lesions might be expected. Then, the histone proteins would act as radiation sensitizers.[4]

Previous EPR results thus suggest electron transfer from the histone to DNA as the prominent consequence of the complex formation between the protein and DNA. Studies using other techniques complement these results. Barton and co-workers have in a series of papers shown that whereas the proteins may shield DNA from external oxidative damage, once oxidation is trapped within DNA no further electron transport between the protein and DNA usually takes place (although exceptions may occur).[12,13]

EPR and the adjunct electron nuclear double resonance (ENDOR) techniques applied to irradiated well-defined single crystal systems are uniquely suited for detailed characterizations of primary radiation induced radical products and their transfer and conversion processes. This permits a molecular-level understanding of radiation-induced processes not easily accessible using other methods.[1] Characteristic features of the nucleosome DNA−protein interactions are known to considerable extent.[14] If these could be modeled in relatively simple crystalline systems, then that would allow for studies directed toward the detailed understanding of the radiation behavior of DNA−histone complexes. Examples of such models system would be hydrogen bonded complexes of an amino acid or dipeptide with a nucleic acid constituent. However, the literature contains very few examples of such complexes which have been well characterized structurally.[15−17] Evidently, the small number is due to the inherent difficulty of preparing crystals of complexes with constituents exhibiting significantly different physiochemical properties. The present work is a report of our first attempt in this direction. Crystals of the complex between *N*-formylglycine and cytosine (C·NFG, Scheme 1) were successfully prepared and investigated after radiation exposure at 10 K or higher temperatures.

The binding motif depicted in Scheme 1 has the C-terminal end of the dipeptide associated with the cytosine base; thus, this is not a major type of association in histone/DNA complexes. Nevertheless, other factors contribute to make this a good starting point. The radiation chemistry of cytosine in a variety of environments is well-known,[1,18−24] as is the basic radiation chemistry of simple amino acid and dipeptides.[25] The crystal structure of NFG was recently solved,[26] and EPR/ENDOR studies of crystalline NFG have been made.[27] Hence, the basic radiation responses of each of the components are well-known providing good prospects for isolating and identifying processes solely depending on the interaction of the two components.

2. Methods

2.1. Crystallography. Cytosine (C) and *N*-formylglycine (NFG) was obtained from Sigma-Aldrich and Fluka. Nearly saturated aqueous solutions of equimolar amounts of C and NFG were prepared at 35 °C. Upon slow cooling to room temperature with subsequent evaporation at this temperature, suitable crystals were collected. A similar procedure was followed to obtain crystals from D_2O (Sigma-Aldrich, 99%) solutions. Here, the easily exchangeable protons (bonded to nitrogen and oxygen) are exchanged with deuterons.

Single crystals of C·NFG are orthorhombic with space group $Pna2_1$.[15] The crystallographic axes were used as reference axes in this study. The unit cell consists of four asymmetric units, interconnected by hydrogen bonding. The asymmetric unit consists of a C·NFG complex as shown in Scheme 1 and Figure 1a. A view of the unit cell down the perpendicular to one set of cytosine bases is shown in Figure 1b. The complex is formed by two hydrogen bonds between the amino acid and the pyrimidine base, $N_4-H\cdots O_3$ and $N_3-H\cdots O_4$, the latter indicating that the cytosine base has become protonated at N3 in this structure with the proton being provided by the carboxyl group. Thus, the *N*-formyl amino acid formally carries a net negative charge while the cytosine base formally carries a net positive charge. All crystals used were examined using X-ray diffraction methods, and the cell parameters agreed well with the published data.[15]

2.2. Room-Temperature Experiments. The crystals were irradiated at 275 K using X-rays from a Philips chromium-target tube operated at 60 kV and 30 mA. Each sample received a total dose of 70 kGy at a rate of about 20 kGy/h as determined by EPR/alanine dosimetry. Through the use of X-ray diffraction, the axis of rotation to be used for the EPR/ENDOR experiments was aligned parallel with one of the crystal axes to within 0.5°. The irradiated crystal was then transferred to a quartz rod without loss of alignment. The quartz rod is a part of a one-axis goniometer allowing for rotation of the sample through 360° to an accuracy of 0.1°.

The EPR spectra were recorded at 295 K using an X-band Bruker ESP300E spectrometer. The measurements were made upon rotating the sample through 5° intervals over 180° around each of the three crystallographic axes. The major part of the experiments was performed using crystals prepared from H_2O, but one complete plane (rot⟨*c*⟩) was also recorded using partially deuterated crystals. ENDOR from samples irradiated at 275 K was not achieved.

2.3. Low-Temperature Experiments. Through the use of X-diffraction techniques, the crystals were aligned along a given axis of rotation (three axes, ⟨*a*⟩, ⟨*c*⟩, and a skewed axis located 50.5° from ⟨*c**⟩ in the ⟨*ac*⟩-plane) were used. This procedure enabled four independent planes of data to be used for analysis and also resolved the Schonland ambiguity in the hyperfine coupling tensors.[28] Details of the experimental procedures including instrumentation, X-ray diffraction, X-irradiation at about 10 K to doses up to about 70 kGy and K-band EPR, ENDOR, and ENDOR-induced EPR (EIE) measurements at 10 K were as previously described.[29,30] The major part of the experiments was performed using partially deuterated crystals, but one complete plane (rot⟨*c*⟩) was also recorded using crystals prepared from H_2O.

2.4. Data Analysis and Computational Methods. The program MAGRES was used to derive the proton hyperfine coupling (hfc) tensors from the ENDOR data.[31] A six-parameter linear regression routine generates initial tensors from the polar angles of the rotation axes, the measurement angle α, and the

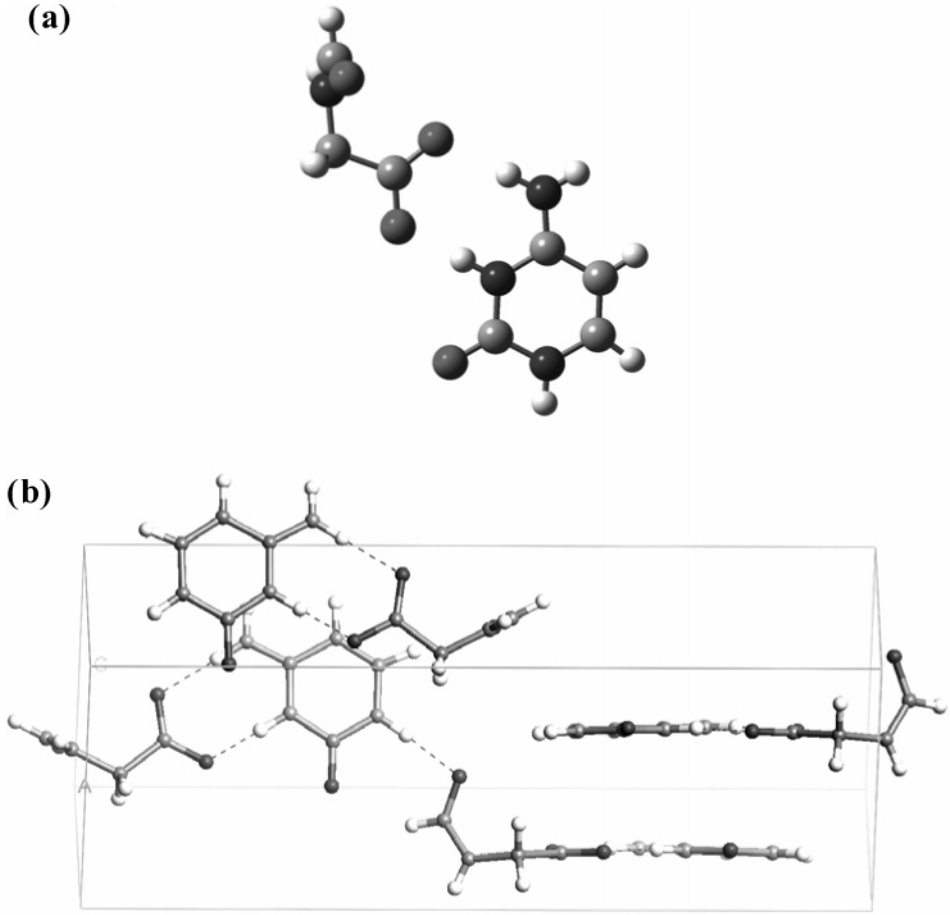

Figure 1. (a) Cytosine·*N*-formylglycine complex viewed down the perpendicular to the cytosine base (0.7749;−0.0330;−0.6312). (b) The cytosine·*N*-formylglycine crystal structure viewed down the same direction for two of the four complexes in the unit cell.

corresponding ENDOR frequency. Refinements also including optimizations of a total of nine angles (polar angles (θ, ϕ) of the rotation axis and the starting value of α of each plane of rotation) were made, using a nonlinear procedure converging to a minimum root-mean-square (rms) value for the complete data set. Providing conservative estimates for the measurement uncertainties, error analyses were made using the method of propagation of errors[31,32] yielding standard errors to the principal values of the hfc tensors and to the components of the corresponding eigenvectors.

Spectrum simulations were made using the program KVASAT as described previously.[33] Crystallographic coordinates were calculated using a modified version of the crystallographic data program ORFEE.[34] The DFT calculations were performed using the GAUSSIAN98 program package.[35] The single-point calculations used the B3LYP hybrid functional and the 6-311+G(2df,p) basis set based on structures optimized using the 6-31+G(d) basis set with a starting geometry obtained from the X-diffraction data,[15] unless stated otherwise explicitly. In combination with the *NoSymm* option of GAUSSIAN98, the eigenvectors (principal directions) of the calculated dipolar coupling principal values are directly comparable with the experimental results.

3. Low-temperature Irradiations

3.1. Experimental Results and Analyses. Immediately after irradiation at about 10 K, clear evidence for three distinct radicals was found, two of which dominated the spectra at all orientations. The third species yielded a weak ENDOR response and could only partly be analyzed. In addition, a few very weak traces of other species were observed exhibiting a far too low yield for analysis and identification. Figure 2a shows the EPR spectrum from a partially deuterated crystal obtained with the external magnetic field directed along $\langle b \rangle$, and Figure 3 shows the corresponding ENDOR spectrum obtained by observing the radio frequency (rf)-induced desaturation of the EPR line marked with an arrow in Figure 2a.

The ENDOR spectra showed clearly the presence of five nonexchangeable proton hyperfine interactions, denoted 1−5 in Figure 3. In crystals prepared from H_2O, only one small and exchangeable interaction could be observed in addition to these resonance lines. This exchangeable coupling never exceeded 5 MHz in magnitude and was too weak for further analysis. Parts b and c of Figure 2 show the EIE spectra obtained by locking the radio frequency to ENDOR transitions marked 1 and 4, respectively, in Figure 3, and sweeping the magnetic field. The EIE experiments clearly showed that ENDOR lines 1, 2, and 3 are due to hyperfine interactions in one radical, denoted R1, whereas lines 4 and 5 both yielded fairly similar doublet patterns, indicating that they are due to two different radicals species both exhibiting mainly one major hyperfine interaction each. These radicals have been denoted R2 and R3. The hyperfine coupling tensors obtained by a full analysis of couplings 1−5 are presented in Table 1.

The anisotropies of couplings 1, 2, and 3 are all characteristic of α-type proton interactions. The isotropic values of couplings 1 and 2 are very similar in magnitude. Furthermore, for couplings 1 and 2, the eigenvectors for the two numerically smallest principal values (expected to occur along the C−H bond directions) make an angle of 126°, whereas the eigenvectors

TABLE 1: Experimental Hyperfine Coupling Tensors (MHz) for Radicals R1−R3 in Single Crystals of Cytosine·*N*-Formylglycine X-irradiated and Measured at 10 K[a]

radical	tensor	isotropic value	principal value	eigenvectors ⟨*a*⟩	eigenvectors ⟨*b*⟩	eigenvectors ⟨*c*⟩
R1 (NFG)	1 (C8−H_a)	−47.84 (3)	−77.38 (4)	−0.156 (1)	0.640 (1)	−0.752 (1)
			−45.64 (4)	0.550 (0)	0.689 (1)	0.472 (1)
			−20.48 (7)	0.820 (0)	−0.340 (1)	−0.460 (1)
	2 (C8−H_b)	−49.94 (4)	−80.53 (8)	−0.740 (1)	0.668 (1)	−0.076 (1)
			−48.86 (7)	0.592 (1)	0.701 (1)	0.398 (1)
			−20.43 (7)	−0.319 (1)	−0.250 (1)	0.914 (1)
	3 (C9−H)	−13.17 (13)	−19.87 (24)	0.623 (2)	−0.139 (2)	−0.770 (1)
			−13.34 (23)	0.674 (2)	0.594 (1)	0.439 (1)
			−5.30 (20)	0.396 (1)	−0.793 (2)	0.464 (1)
R2[b] (Cyt)	4 (C6−H)	−38.6	−65.0	−0.5782	0.3660	−0.7292
			−32.2	0.7749	−0.0330	−0.6312
			−18.6	0.2553	0.9300	0.2643
R3[c] (Cyt)	5 (C6−H)	−33.8	−49.2	−0.5782	0.3660	−0.7292
			−37.1	0.7749	−0.0330	−0.6312
			−15.1	0.2553	0.9300	0.2643
crystallographic directions for C·NFG:						
normal to plane N5−C9−H(C9)				0.6533	0.4756	0.5891
normal to plane C5−C6−N1				0.7749	−0.0333	−0.6312
C9−H(C9)				0.4096	−0.8764	0.2533
C6−H(C6)				0.2853	0.9280	0.2395
C8−H($C8_a$)[c]				0.7569	−0.4298	−0.4923
C8−H($C8_b$)[c]				−0.3949	−0.4497	0.8011

[a] Radical R1 is shown in Scheme 2, and radical R2 is shown in Scheme 3. There are four molecular sites in the unit cell. If a given direction (*l*,*m*,*n*) in the table is associated one given molecular site, the corresponding direction in the other three will be given by (*l*,*m*,−*n*), (*l*,−*m*,*n*), and (−*l*,*m*,*n*). [b] See text for how these coupling tensors were derived. [c] Calculated using the perpendicular to the N5−C9−H9 plane and the N5−C8 bond direction assuming sp^2 hybridization at C8.

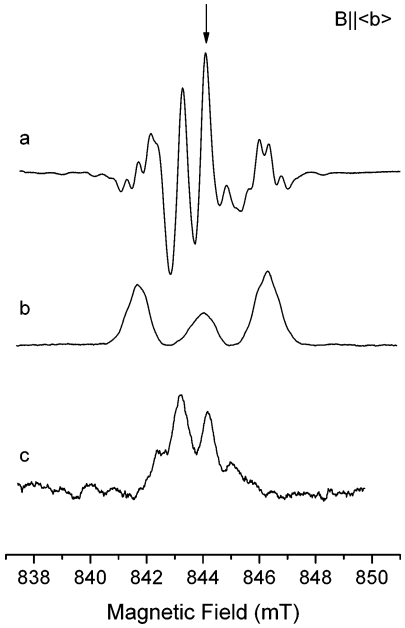

Figure 2. (a) Second derivative EPR spectrum of a partially deuterated cytosine·*N*-formylglycine crystal irradiated at 10 K measured with the magnetic field directed along ⟨*b*⟩. The arrow indicates the field position for the ENDOR spectrum in Figure 3. The microwave frequency is 23 623.71 MHz. (b) EIE spectrum obtained by locking the radio frequency to ENDOR line positions 1, 2, and 3 in Figure 3. (c) EIE spectrum obtained by locking the radio frequency to the ENDOR position 4 in Figure 3.

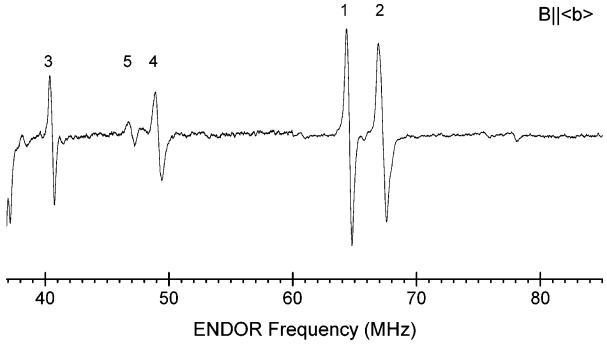

Figure 3. ENDOR spectrum of a partially deuterated cytosine·*N*-formylglycine crystal irradiated at 10 K measured with the magnetic field directed along ⟨*b*⟩ and at the value marked by an arrow in Figure 2. The different ENDOR lines are marked with numerals 1−5. The free proton frequency was 35.95 MHz.

SCHEME 2. Radical R1

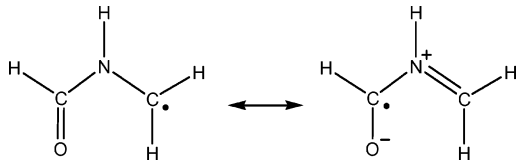

for the two intermediate principal values (being directed along the lone electron orbital (LEO)) are parallel to within 5°. These features are characteristic for a sp^2-hybridized $^{\bullet}CH_2$ radical fragment. Considering possible candidates for such a fragment in the present system, only a decarboxylated NFG radical fragment fitted the experimental data, as indicated by comparing expected bond directions for the two remaining C8−H bonds (calculated from crystal data coordinates) with the eigenvectors for the two numerically smallest principal values for couplings 1 and 2 (see Table 1). Coupling 3 is safely associated with the proton at C9 from similar arguments. Here, the numerically minimum principal value occurs in a direction less than 13° from the crystallographic C9−H bond whereas the direction for the intermediate principal value is about 10° from the perpendicular to the N5−C9−H9 fragment.

These results indicate that the radical structure responsible for this resonance is that depicted in Scheme 2, a decarboxylated *N*-formylglycine species.

The radical is basically a conjugated π-electron species. The atomic $2p_z$ orbital spin densities may be estimated from the anisotropic coupling elements using the Bernhard−Gordy relations[36] to 0.71, 0.76, and 0.18 for couplings 1, 2, and 3, respectively. Alternatively, from the McConnell relation[37] with

SCHEME 3. Radical R2

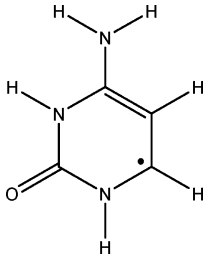

$Q = -72$ MHz, the corresponding numbers are 0.67, 0.69, and 0.18. The fairly good agreement between these two sets of numbers indicates a structure that is close to planar but perhaps with a slight and asymmetric bending at the methylene fragment.[38]

ENDOR lines 4 and 5 were easily followed in the rot⟨*c*⟩ plane and, for coupling 4, also in the rot⟨*a*⟩ plane. Unfortunately, in the third plane of rotation, the ENDOR lines were too weak to be followed. However, the available data for line 4, including the few data points in the third plane, could be perfectly reproduced assuming an α-proton hyperfine coupling tensor. Indeed, the eigenvectors associated with a planar α-proton coupling are uniquely defined by the C−H bond direction, the direction of the lone electron orbital (being perpendicular to the C− H bond), and a third direction perpendicular to both of these two. Then, choosing such orthogonal eigenvectors associated with the C6−H fragment of the cytosine base, a set of principal values could be found so that the calculated coupling at each specific orientation fitted all the corresponding experimental data closely. The available data furthermore show that line 5 closely follows line 4 where it is observable. Thus, scaling down the principal elements of coupling 4 while retaining the eigenvectors also resulted in a hfc tensor that gave a very good fit to the available data for line 5. The hyperfine coupling tensors associated with resonance lines 4 and 5 are given in Table 1. The EIE experiments showed that these are due to two different radicals R2 and R3, each showing a doublet EPR pattern with a splitting corresponding to ENDOR lines 4 and 5, respectively.[39]

The hyperfine couplings arrived at for R2 and R3 are typical for those from the one-electron reduced cytosine species. The N3-protonated, one-electron reduced cytosine radical has been detected in a large number of cytosine derivatives such as cytosine monohydrate,[30] cytosine hydrochloride,[20] 2′-deoxycytidine hydrochloride,[22] deoxycytidine 5′-monophosphate,[40] and cytidine 3′-phosphate.[41] They are all practically indistinguishable from those of R2 in Table 1. Thus, it is proposed that R2 is the neutral, N3-protonated one-electron reduced planar cytosine base radical as shown in Scheme 3.

The less abundant radical R3 exhibits a H(C6) coupling whose principal values are systematically smaller than those of radical R2. The apparent occurrence of several slightly different versions of the one-electron reduction products is a common feature of cytosine derivatives and usually ascribed to different geometric conformations or different protonation states of the radical.[42,43] In the present case, the available experimental data are insufficient to establish a plausible identification of R3.

3.2. Low-Temperature Simulations. Figure 4 shows the results of simulations of the EPR spectra due to radicals R1−R3, using the KVASAT program[33] and the parameters given in Table 1 obtained from partially deuterated crystals of the complex. Relative *g* values and line widths were estimated from the experimental spectra. For an acceptable simulation of R1, however, one small nitrogen coupling had to be included for this radical. Best results were obtained using a nitrogen coupling of 5.6 MHz for the orientation depicted in Figure 4; B||⟨*b*⟩. Simulating spectra at a few other orientations with well-resolved spectra showed that a similar nitrogen coupling always had to be included and that this coupling is not very anisotropic. For instance, the ⟨*a*⟩-axis spectrum was best simulated with a nitrogen coupling of 7.3 MHz (not shown). In the calculated spectrum in Figure 4, the simulated spectra due to each of the radicals R1−R3 were added in a relative weight of 0.78:0.15:0.07, respectively.

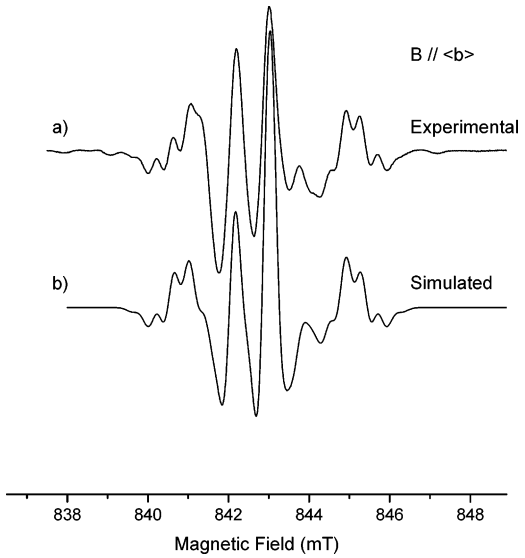

Figure 4. (a) Same as Figure 2a. (b) Simulated ⟨*b*⟩-axis spectrum using the hyperfine coupling tensors for radicals R1, R2, and R3 given in Table 1. An additional nitrogen hyperfine interaction of 5.6 MHz was added for R1. The *g* value for R2 was shifted 0.0011 up from that of R1, whereas the *g* value of R3 was shifted 0.0008 correspondingly. The relative weights of the three resonances were 0.78:0.15:0.07

The results in Figure 4 show that the parameters extracted for R1 and R2/R3 are able to reproduce the major features of the experimental low-temperature spectra from partially deuterated crystals.

3.3. DFT Calculations. Model calculations were performed on the full C·NFG asymmetric unit and additional separate calculations were made for each of the structures designated R1 and R2. Crystallographic coordinates were used throughout. For R1, the CO_2^- residue was removed from the isolated NFG anion, and the resulting neutral radical was optimized using B3LYP/6-31+G(d), and the subsequent single-point calculation was made using the B3LYP/6-311+G(2df,p) basis set. For R2, the nonoptimized anionic structure of the full complex (comprising the N3-protonated cytosine cation) was taken as the starting point for a B3LYP/6-311G(2df,p) single-point calculation. In this case, geometry optimizations were not done to avoid the previously reported effects of bending of the cytosine reduction radicals in the gas phase.[44] The results are presented in Table 2. Since the *NoSymm* option was used, the eigenvectors for the calculated dipolar couplings could be compared directly with the corresponding experimental eigenvectors, the angles of deviation are given in a separate column (φ). The overall agreement between calculated and experimental results is very good, including the estimated nitrogen coupling deduced from the spectral simulations.

4. Room-temperature Irradiations

4.1. Experimental Results and Analyses. First derivative EPR spectra from a H_2O-grown crystal X-irradiated at 275 K

TABLE 2: DFT Calculated Hyperfine Coupling Tensors (MHz) and *g* tensors for Radicals R1 and R2 in Single Crystals of Cytosine·*N*-Formylglycine X-irradiated and Measured at 10 K[a]

				eigenvectors			
radical	tensor	isotropic value	principal value	⟨*a*⟩	⟨*b*⟩	⟨*c*⟩	φ^b
			−85.50	−0.0476	0.7244	−0.6877	8.8
	1 (C8−H_a)	−53.60	−52.68	0.5886	0.5766	0.5666	8.7
			−22.65	0.8070	−0.3778	−0.4539	2.6
			−87.75	−0.6822	0.7303	−0.0354	5.5
	2 (C8−H_b)	−54.00	−52.32	0.5880	0.5767	0.5672	12.0
			−21.93	−0.4346	−0.3662	0.8228	10.8
			−14.66	0.7335	−0.0872	−0.6740	9.9
	3 (C9−H)	−9.43	−11.29	0.5888	0.5768	0.5662	8.8
			−2.34	−0.3394	0.8122	−0.4745	3.0
R1 (NFG)							
			−7.96	0.7469	−0.1200	−0.6541	
	N5	−4.23	−7.00	−0.3092	.8081	−0.5014	
			−2.24	0.5887	.5767	0.5664	7.0[c]
			−9.60	−0.1431	−0.6155	0.7750	
	H(N5)	−5.14	−9.23	0.5880	0.5770	0.5669	
			3.43	0.7961	−0.5368	−0.2793	
			2.0038	−0.3273	−0.4667	0.8216	
	g	2.0031	2.0033	−0.7421	0.6652	0.0821	
			2.0022	0.5859	0.5829	0.5641	
			−66.12	0.5815	−0.3712	0.7239	3.8
R2 (Cyt)	4 (C6−H)	−37.11	−30.92	0.7569	−0.0796	−0.6487	3.0
			−14.25	0.2985	0.9251	0.2347	3.0
crystallographic directions for C·NFG:							
normal to plane N5−C9−H(C9)					0.6533	0.4756	0.5891
normal to plane C5−C6−N1					0.7749	−0.0333	−0.6312
C9−H(C9)					0.4096	−0.8764	0.2533
C6−H(C6)					0.2853	0.9280	0.2395
C8−H($C8_a$)[d]					−0.7569	0.4298	0.4923
C8−H($C8_b$)[d]					0.3949	0.4497	−0.8011

[a] See footnote 3 in Table 1. [b] Angle with the corresponding experimental direction in Table 1. [c] This is the angle with the perpendicular to the plane N5−C9−H9. [d] Calculated using the perpendicular to the N5−C9−H9 plane and the N5−C8 bond direction assuming sp^2 hybridization at C8.

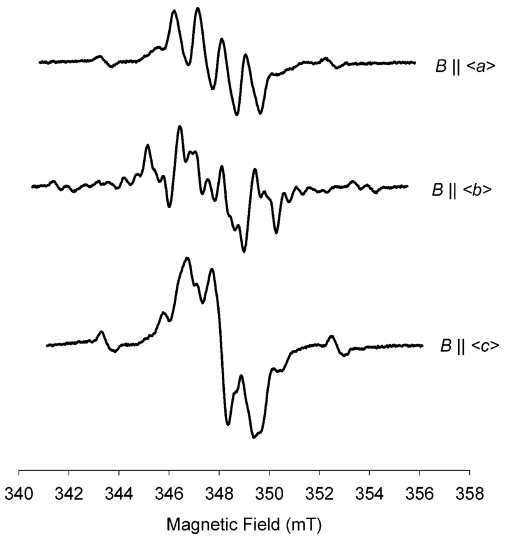

Figure 5. First derivative EPR spectra of H_2O grown cytosine·*N*-formylglycine crystals irradiated at 275 K and measured at 293 K with the magnetic field directed along the three crystallographic axes, as indicated. The *g* values of the central resonances are 2.0032, 2.0034, and 2.0036, respectively.

obtained with the magnetic field along each of the three crystallographic axes are shown in Figure 5. The spectra exhibit strong features in the center varying from a poorly resolved triplet (B||⟨*c*⟩) through a quartet of triplets (B||⟨*b*⟩) to a well-resolved quartet (B||⟨*a*⟩). These are characteristics not previously observed in any cytosine base derivative and are hence ascribed to a radical in the NFG moiety. Weaker features on the wings, however, are characteristic for the cytosine hydrogen-addition radicals.[1] The strong central features are ascribed to a radical henceforth designated as R4. Also, the weak outer lines from the cytosine hydrogen adducts are visible only in very limited regions of the plane. The two H-adducts of N3-protonated cytosine are designated R5 and R6 (see below).

It was not possible to obtain ENDOR signals from these room-temperature irradiated crystals. Thus, the spectral analysis was done using the EPR spectra alone. For the R1 resonance, two proton doublets and a nitrogen triplet coupling characterizes the strong features of the spectra. The largest and most anisotropic proton coupling exhibits a maximum value close to ⟨*b*⟩, while the smallest width of the spectra is along ⟨*c*⟩. Here, the two proton couplings are of comparable magnitude and the nitrogen coupling is not resolved. Even if poorly expressed site-splitting complicates the spectra at most orientations, it was possible to extract hyperfine coupling tensors for the two proton interactions. However, for the nitrogen coupling, only estimates at selected orientations could be made. Table 3 shows the hyperfine coupling parameters for R4 as extracted from the available EPR data. For the α-type coupling **1**, the spin density at the central carbon atom is estimated to 0.76 both from the isotropic and dipolar coupling parameters.[36,37]

Considering possible candidates for the R4 radical, only the well-known glycine backbone radical (Scheme 4) could be made to fit the data. From the crystallographic data, the eigenvector for the numerically minimum value of coupling 1 deviates 37° from the calculated C8−H bond direction. There is a similar deviation between the normal to the C7−C8−N5 fragment and the intermediate principal value, expected to be parallel to the lone electron orbital (LEO).[1] It was considered whether these deviations from the crystal molecular structure possibly could be due to a rotation of about 38° about the N5−C8 bond upon

TABLE 3: Experimental (EPR only) Hyperfine Coupling Parameters (MHz) for the Central Resonance R4[a] in Single Crystals of Cytosine−*N*-formylglycine, Irradiated and Measured at Room Temperature[b]

				eigenvectors		
radical	tensor	isotropic value	principal values	⟨*a*⟩	⟨*b*⟩	⟨*c*⟩
R4 (NFG)	**1** (C8−H)	−55.60 (2)	−85.2 (3)	0.071 (28)	−0.996 (3)	−0.046 (28)
			−52.4 (2)	0.995 (2)	0.074 (28)	−0.068 (24)
			−29.2 (4)	0.072 (24)	−0.041 (28)	0.997 (2)
	2 (N5−H)	30.7 (1)	38.1 (2)	0.002 (83)	−0.983 (3)	−0.186 (376)
			27.9 (2)	1.000 (12)	0.003 (101)	−0.007 (66)
			26.2 (2)	0.008 (66)	−0.186 (372)	0.983 (13)
	3 N5	≤10	near isotropic		maximum value close to ⟨*b*⟩	
crystallographic directions for C·NFG:						
normal to plane to C7−C8−N5				0.7512	0.0752	−0.6558
normal to planet N5−C9−H(C9)				0.6533	0.4756	0.5891
normal to cytosine ring				−0.7749	0.0333	0.6312
N5−H(N5)				−0.7380	0.4207	0.5276
C8−H(C8)[3]				0.6601	−0.0988	0.7447
C8···H(N5)				−0.5683	0.8227	0.0153
C9−H(C9)				−0.4096	0.8764	−0.2533
C9···H(N5)				−0.5913	−0.1431	0.7937

[a] Radical R4 is shown in Scheme 4. [b] See footnote *a* in Table 1. [c] Calculated from the sum of vectors C7−C8 and N5−C8.

SCHEME 4. Radical R4

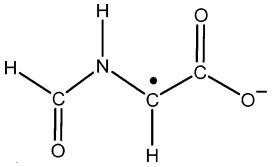

SCHEME 5. Radical R5 and Radical R6

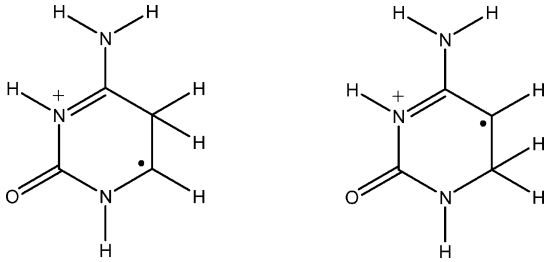

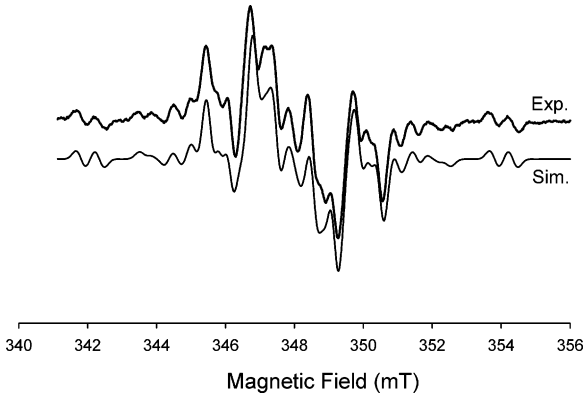

Figure 6. Experimental and simulated first derivative ⟨*b*⟩-axis EPR spectra of a H_2O grown cytosine·*N*-formylglycine crystal irradiated at 275 K and measured at 293 K. For details on the simulated spectrum, see text.

radical formation. Support for this was found by the following consideration:

Coupling 2 (Table 3) is a β-type coupling, most probably due to H(N5). From the crystallographic data, the dihedral angle of the N5−H bond with respect to the normal to the plane C7−C8−N5 is 171°. Using the Heller−McConnell relation[45]

$$a_{\mathrm{iso}}{}^{\beta} = (B_0 + B_2 \cos^2 \theta)\rho^{\pi}$$

with $B_0 = -4.3$ MHz, $B_2 = 117.6$ MHz,[46] and $\rho^{\pi} = 0.76$, a value for $a_{\mathrm{iso}}{}^{\beta}$ of 83.8 MHz is obtained, far larger than that observed. However, the required rotation of 38° about the C−N bond reduces the dihedral angle to 128° and consequently the coupling to 31 MHz (exptl value 30.7 MHz). Further support for this proposed molecular reorientation was obtained from DFT calculations (see below).

The cytosine hydrogen-addition radicals are well-known from the literature[1] and hence do not warrant detailed descriptions; here, it suffices to refer to Figure 5. The C6 H-addition radical (see Scheme 5, radical R6) typically exhibits two β-couplings totaling about 280 MHz (about 10 mT) and a α-coupling due to about 70% spin at C5. This fits nicely with the wide spectrum observed for B ||⟨*b*⟩ in Figure 5. The extra small splitting is most probably due to an additional coupling to one of the amino protons.[23] Observing the smallest line widths along ⟨*b*⟩ agrees with previous observations that the maximum nitrogen coupling occurs along the normal to the cytosine plane for this radical.[47] The ⟨*b*⟩-axis is in the ring plane (perpendicular to the ring plane).

The C5 H-addition radical (see Scheme 5, radical R5) is characterized by somewhat smaller β-couplings (sum typically 200 MHz or about 7 mT) and a α-coupling similar in magnitude to that of the C6 hydrogen adduct. The nitrogen coupling typically exhibits a near-zero value with the field along the ring normal due to spin-polarization effects. The ring normal is perpendicular to ⟨*b*⟩, and the C5 H-adduct should thus be most easily seen along ⟨*a*⟩ and ⟨*c*⟩.

4.2. Room-temperature Simulations. The room-temperature EPR spectra were successfully simulated using spectral parameters for R4, R5, and R6 as discussed above, assisted by literature values for the cytosine hydrogen-addition radicals R5 and R6. This is illustrated for the ⟨*b*⟩-axis spectrum in Figure 6. However, to obtain this simulation, and also those at all other orientations, a broad singlet structure with a line width of about 40 MHz (1.5 mT) had to be included. Similar singlet resonances have previously been observed in several crystalline cytosine systems[48] and are so far only tentatively ascribed to various unidentified room-temperature cytosine radicals. The relative contributions of the various radicals typically were of the order 40% R3, 5−8% of each of R4 and R5, and 50% of the singlet.

4.3. MO Calculations. DFT calculations aimed at understanding the structure of the R4 radical were made. For these

TABLE 4: Calculated Hyperfine Coupling Parameters (MHz) for the Two Structures I and II (see text) of Radical R4 in Single Crystals of Cytosine−*N*-formylglycine X-irradiated and Measured at Room Temperature[a]

coupling		I	II	exp
1 (C8−H)	(isotropic)	−55.8	−49.0	−55.6
	(dipolar)	−36.2	−32.5	−26.4
		−0.7	−0.1	−3.2
		36.9	32.6	29.4
2 (N5−H)	(isotropic)	79.6	34.8	30.7
	(dipolar)	10.1	6.8	7.3
		−3.9	−1.0	−2.8
		−6.2	−5.8	−4.5
3 N5	(isotropic)	−9.5	−5.6	(−)10.2[b]
	(dipolar)	0.6	2.4	3.2[b]
		0.1	−0.8	−1.6
		−0.7	−1.6	−1.6

[a] Experimental data from Table 3 are given for comparison. [b] Estimated parameters from a few data points only.

calculations, an isolated NFG molecule with one of the H(C(8)) atoms removed was used. First, an optimized structure (I) based on crystallographic coordinates but with two torsion angles (the H(N5)−N5−C8−C9 and C9−N5−C8−C7 angles) frozen was used for a reference calculation. Fixing these two torsion angles was necessary to avoid a complete planarization of the molecule upon geometry optimization. Next, an optimized structure where the torsion angle around the N5−C8 bond was increased by 38° and then frozen was made (II). The major results from these two calculations are given in Table 4. It appears that the rotated structure II yields results in good agreement with the experimental data.

5. Mechanistic Aspects

5.1. Experimental Results. Upon warming from 10 K, the anion resonances R2 and R3 are lost at about 100 K. At room temperature, weak traces of the cytosine hydrogen-addition radicals (R5, R6) are observed, but it was not possible to establish any clear connection between the disappearance of the R2 and R3 species and the formation of the cytosine H-adducts R5 and R6.

The resonance due to the R1 radical is gradually lost upon warming above 150 K. The resonance due to radical R4 grows in slowly at about the same temperature. Although no detailed kinetics study was performed, the present results indicate that the two processes are connected.

5.2. MO Calculations. The experimental results obtained after low-temperature irradiations indicate that a separation of oxidation and reduction products between the amino acid and the cytosine base residues, respectively, takes place. To investigate the possibilities for such a separation of processes, which must imply hole transfers from the cytosine base to the NFG residue, and a preferred trapping of electrons at the cytosine residue, DFT calculations were performed with the objective to obtain ionization potentials and electron affinities for the two sub-systems.

Accurate ionization potentials (IPs) were obtained using ab initio propagator calculations in the partial third-order (P3) approximation with the 6-311G(d,p) basis set.[49] The results are −14.13 eV for cytosine protonated at N3 and −4.43 eV for NFG with the negatively charged CO_2 group. These results indicate that NFG will be more easily oxidized than protonated cytosine in this cocrystal. Electron affinities (EAs) have been calculated first using B3LYP/6-31+G(d,p) to optimize the geometries of cytosine and NFG and then single-point calculations at the B3LYP/6-311+G(2df,p) level on the optimized species. The results are +4.79 eV for the N3-protonated cytosine and −4.35 eV for NFG. These results, being summarized in Table 5, indicate that protonated cytosine will be the best electron trap. The negative EA for NFG indicates that it requires energy to add an electron to an anion.

TABLE 5: DFT Calculated Electron Affinities and Ionization Potentials (eV) for the Components of the C·NFG Complex[a]

	NFG(CO_2^-)	C(+HN_3)
electron affinity	−4.35	+4.79
ionization potential	−4.43	−14.13

[a] The NFG molecule has donated a proton to the cytosine N3 (see Scheme 1).

SCHEME 6. Decarboxylation of the Neutral *N*-Formylglycine Oxidation Product

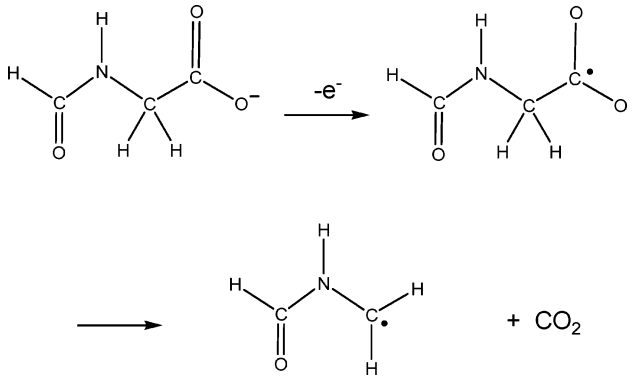

The experimental results suggest that radical R1 is a decarboxylated NFG oxidation product (see Discussion section). Removing such a large molecular fragment from the primary oxidation product may seem difficult at these low temperatures. Thus, attempts were made to model the decarboxylation process using DFT calculations as follows: B3LYP/6-31+G(d) calculations were made on the optimized neutral NFG and on the separate products (the $\cdot CH_2-NH-CHO$ radical and the CO_2 fragment). The fragments gain 19.42 kcal/mol upon separation. Since the calculations were done on the geometry optimized fragments, some of this energy gain is from reorganization. It was further shown that the reaction was energetically all downhill by removing the CO_2 fragment from the NFG in 0.05 Å increments of the C−C bond.

It thus appears that decarboxylation of the NFG one-electron oxidation product is a barrier-free process that will occur spontaneously after the oxidation process, as illustrated in Scheme 6.

6. Discussion

The primary ionization, that is, the radiation provoked ejection of an electron, will occur stochastically throughout the sample, only weighted by the number of valence electrons at each atomic position. Thus, both the NFG residue and the cytosine residue will become ionized in an almost random proportion. The present low-temperature EPR/ENDOR data reveal no evidence for oxidation at the cytosine base. An efficient transfer of holes from the cytosine base to the NFG residue consequently took place. The oxidation potential of the deprotonated NFG residue is far lower than the oxidation potential of the N3-protonated cytosine base (Table 5) constituting a strong driving force for the hole transfer.

The most common degradation product of the amino acid cation is formed by decarboxylation.[25] Decarboxylation of one-

SCHEME 7. Formation of the Amino Acid Backbone Radical

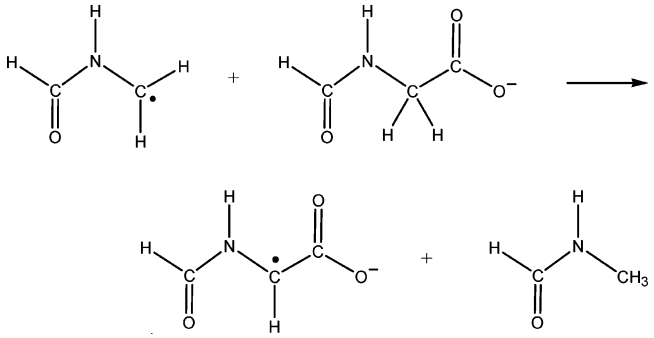

electron oxidized amino acids invariably takes place even at very low temperatures indicating a very low, or zero, activation energy barrier for the process. Eriksson et al.[50] showed using DFT calculations that decarboxylation from the L-*o*-serinephosphate cation was a barrier-free process. The calculations reported in the present work for the NFG cation yield similar results. These considerations provide a good basis for understanding the observation that radical R1 is the only observable oxidation product at 10 K.

In amino acids, the decarboxylation radical commonly abstracts a hydrogen from a neighboring molecule forming the so-called backbone radical, the radical formed by hydrogen abstraction from the α-carbon, as depicted in Scheme 7:

The observation of radical R4 at room temperature suggests that similar processes take place in the C·NFG complex.

The electrons ejected upon the primary oxidation event will predominantly become trapped at those sites exhibiting the largest electron affinity. If initial trapping takes place at other sites, the differences in electron affinity will constitute a driving force for the transfer of the electron to the site with the largest electron affinity. According to the results in Table 5, this site is the N3-protonated cytosine base. In the present crystal matrix, there are apparently two energetically similar versions (with respect to geometry or protonation state) of this one-electron reduced species. The dominant one is the neutral, N3-protonated cytosine anion radical (R2), while the other (R3) could not be identified with any confidence in the present study. The actual mechanisms for the formation of the H-adduct radicals R5 and R6 could not be established, although it seems reasonable that these are connected to the decay of the R2 and R3 species.

The major result obtained in this study is that effective separation of trapped oxidation and reduction products between the two constituents of the C·NFG complex takes place at low temperature, apparently driven by large differences in ionization potentials and electron affinities of each constituent. This experimental result is nicely illustrated by the DFT calculated spin density distributions for the primary anion and cation radicals of the complex shown in Figure 7. Here, isosurfaces of the electron spin density distributions (positive and negative) are obtained from B3LYP/6-311G(2df,p) single-point calculations of the reduction and oxidation products calculated with the unoptimized crystal geometry. The π nature of the anion spin distribution and the σ nature of the cation spin distribution are clearly recognizable. The thermal annealing and room-temperature results furthermore indicate that secondary radical reactions do not change this initial separation of oxidation and reduction products, that is, no further electron or hole transport takes place between the constituents of the complex.

Experimental observations similar to these were also made in a previous study of a complex of cytidine·salicylic acid (cyt·sal).[51] The association motif between the two components in cyt·sal is similar to that in the C·NFG complex, rendering the cytosine base protonated at N3. Considering that this is an EPR study only and hence less detailed with respect to the presence of less abundant components in the spectra, the cyt·sal results nevertheless demonstrated exclusive oxidation at the salicylic acid component (containing the carboxyl group) and that the majority of reduction products were cytosine base radicals.

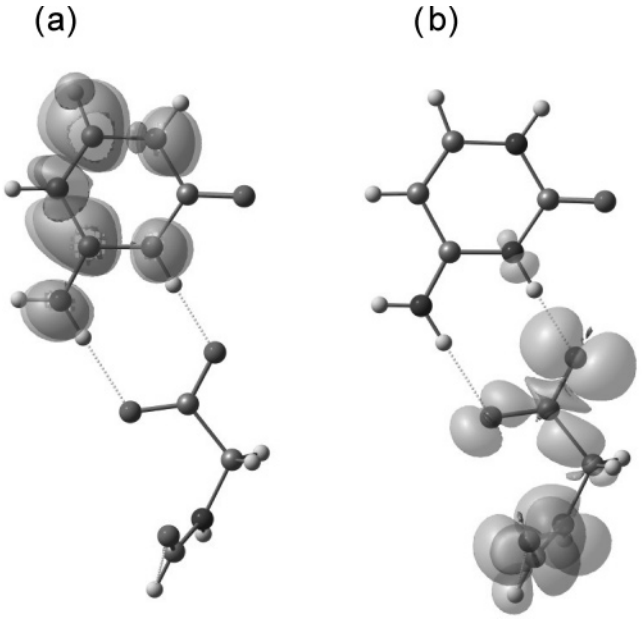

Figure 7. Cytosine-*N*-formylglycine electron spin density isosurfaces at 0.00151 au contour value for (a) the anion radical and (b) the cation radical. Both DFT calculations are B3LYP/6-311G(2df,p) single-point calculations on unoptimized crystallographic geometries.

In the context of DNA−protein complexes, the results obtained in the present work indicate that, upon exposure to ionizing radiation, oxidation will be shifted away from DNA by electron transfer from the protein and the holes will become trapped at protein sites. Furthermore, electrons created by initial oxidation at both the protein and the DNA will become trapped in DNA. This will increase the ratio of anion to cation percentages in DNA in line with the observations of Weiland and Hüttermann.[11] Thus, if it is the oxidative pathway that leads to strand breaks in DNA, then the association with histones will provide an apparent radioprotective effect.[5] However, since the C-terminal association motif of the amino acid with cytosine in the C·NFG complex cannot be highly abundant in DNA−histone complexes,[14] it remains to be seen if more abundant motifs may lead to results as clear as those observed in the present work. Work along these lines is in progress.

Acknowledgment. This work was in part supported by NIH Grant CA36810.

References and Notes

(1) Bernhard, W. A. *Adv. Radiat. Biol.* **1981**, *9*, 199.

(2) Von Sonntag, C. *The Chemical Basis of Radiation Biology*; Taylor and Francis: London, 1987.

(3) Sevilla, M. D.; Becker, D. Radiation damage in DNA. In *Electron Spin Resonance*; Gilbert, B. C., Davies, M. J., Murphy, D. M., Ed.; Royal Society of Chemistry: London, 1994; Vol. 14, p 130.

(4) Bernhard, W. A.; Close, D. M. DNA Damage Dictates the Biological Consequences of Ionizing Irradiation: The Chemical Pathways. In *Charged Particle and Photon Interactions with Matter: Chemical, Physicochemical, and Biological Consequences with Applications*; Mozumber, A., Hatano, Y., Eds.; Marcel Dekker: New York, 2003; p 431.

(5) Sevilla, M. D.; Becker, D. ESR Studies of Radiation Damage to DNA and Related Biomolecules. In *Electron Paramagnetic Resonance*; Gilbert, B. C., Davies, M. J., Murphy, D. M., Eds.; Royal Society of Chemistry: London, 2004; Vol. 19, p 243.

(6) Alexander, P.; Lett, J. T.; Ormerod, M. G. *Biochim. Biophys. Acta* **1961**, *51*, 207.

(7) Lillicrap, S. C.; Fielden, E. M. *Int. J. Radiat. Biol.* **1972**, *21*, 137.

(8) Olast, M.; Bertinchamps, A. J. *Int. J. Radiat. Biol.* **1973**, *24*, 589.

(9) Cullis, P. M.; Jones, G. D. D.; Symons, M. C. R.; Lea, J. S. *Nature (London)* **1987**, *330*, 773.

(10) Faucitano, A.; Buttafava, A.; Martinotti, F.; Pedraly-Noy, G. *Radiat. Phys. Chem.* **1992**, *40*, 357.

(11) Weiland, B.; Hüttermann, J. *Int. J. Radiat. Biol.* **2000**, *76*, 1075.

(12) Nunez, M. E.; Noyes, K. T.; Barton, J. K. *Chem. Biol.* **2002**, *9*, 403.

(13) Yavin, E.; Boal, A. K.; Stemp, E. D. A.; Boon, E. M.; Livingston, A. L.; O'Shea, V. L.; David, S. S.; Barton, J. K. *Proc. Natl. Acad. Sci. U.S.A.* **2005**, *102*, 3546.

(14) Luscombe, N. M.; Laskowski, R. A.; Thornton, J. M. *Nucleic Acids Res.* **2001**, *29*, 2860.

(15) Ohki, M.; Takenaka, A.; Shimanouchi, H.; Sasada, Y. *Bull. Chem. Soc. Jpn.* **1975**, *48*, 848.

(16) Sasada, Y.; Takenaka, A. *Adv. Biophys.* **1988**, *24*, 57.

(17) Görbitz, C. H.; Sagstuen, E. *Acta Crystallogr., Sect. E* **2004**, *60*, 1945−1947.

(18) Close, D. M. *Radiat. Res.* **1993**, *135*, 1.

(19) Hole, E. O.; Sagstuen, E.; Close, D. M.; Nelson, W. H. Protonation/deprotonation processes of primary products in X-irradiated cytosine derivatives: EPR and ENDOR studies at 10 K. In *Radiation Damage in DNA: Structure/Function Relationships at Early Times*; Fuciarelli, A. F., Zimbrick, J. D., Eds.; Battelle Press: Columbus, OH, 1995; p 105.

(20) Hole, E. O.; Nelson, W. H.; Sagstuen, E.; Close, D. M. *Radiat. Res.* **1998**, *149*, 109.

(21) Close, D. M.; Eriksson, L. A.; Hole, E. O.; Sagstuen, E.; Nelson, W. H. *J. Phys. Chem. B* **2000**, *104*, 9343.

(22) Hole, E. O.; Sagstuen, E.; Nelson, W. H.; Close, D. M. *Radiat. Res.* **2000**, *153*, 823.

(23) Krivokapic, A.; Hole, E. O.; Sagstuen, E. *Radiat. Res.* **2003**, *160*, 340.

(24) Sankovic, K.; Malinen, E.; Medunic, Z.; Sagstuen, E.; Herak, J. N. *Phys. Chem. Chem. Phys.* **2003**, *5*, 1665.

(25) Sagstuen, E.; Sanderud, A.; Hole, E. O. *Radiat. Res.* **2004**, *162*, 112.

(26) Görbitz, C. H.; Sagstuen, E. *Acta Crystallogr., Sect. E* **2004**, *60*, 841.

(27) Vågane, R. Energy transfer between histones and DNA. MSc Thesis (in Norwegian), University of Oslo, Oslo, Norway, 2002.

(28) Schonland, D. S. *Proc. Phys. Soc.* **1959**, *73*, 788.

(29) Hole, E. O.; Sagstuen, E.; Nelson, W. H.; Close, D. M. *J. Phys. Chem.* **1991**, *95*, 1494.

(30) Sagstuen, E.; Hole, E. O.; Nelson, W. H.; Close, D. M. *J. Phys. Chem.* **1992**, *96*, 8269.

(31) Nelson, W. H. *J. Magn. Reson.* **1980**, *38*, 71.

(32) Sørnes, A.; Sagstuen, E. *J. Phys. Chem.* **1995**, *99*, 16857.

(33) Sagstuen, E.; Lund, A.; Itagaki, Y.; Maruani, J. *J. Phys. Chem. A* **2000**, *104*, 6362.

(34) Busing, W. R.; Martin, K. O.; Levy, H. A. ORNL-TM-306; Oak Ridge National Laboratories: Oak Ridge, TN, 1964.

(35) Frisch, M. J.; Trucks, G. W.; Schlegel, H. B.; Scuseria, G. E.; Robb, M. A.; Cheeseman, J. R.; Zakrzewski, V. G.; Montgomery, J. A., Jr.; Stratmann, R. E.; Burant, J. C.; Dapprich, S.; Millam, J. M.; Daniels, A. D.; Kudin, K. N.; Strain, M. C.; Farkas, O.; Tomasi, J.; Barone, V.; Cossi, M.; Cammi, R.; Mennucci, B.; Pomelli, C.; Adamo, C.; Clifford, S.; Ochterski, J.; Petersson, G. A.; Ayala, P. Y.; Cui, Q.; Morokuma, K.; Malick, D. K.; Rabuck, A. D.; Raghavachari, K.; Foresman, J. B.; Cioslowski, J.; Ortiz, J. V.; Baboul, A. G.; Stefanov, B. B.; Liu, G.; Liashenko, A.; Piskorz, P.; Komaromi, I.; Gomperts, R.; Martin, R. L.; Fox, D. J.; Keith, T.; Al-Laham, M. A.; Peng, C. Y.; Nanayakkara, A.; Challacombe, M.; Gill, P. M. W.; Johnson, B.; Chen, W.; Wong, M. W.; Andres, J. L.; Gonzalez, C.; Head-Gordon, M.; Replogle, E. S.; Pople, J. A. *Gaussian 98*, revision A.9; Gaussian, Inc.: Pittsburgh, PA, 1998.

(36) Bernhard, W. A. *J. Chem. Phys.* **1984**, *81*, 5928.

(37) McConnell, H. M.; Chesnut, D. B. *J. Chem. Phys.* **1958**, *28*, 107.

(38) Erling, P. A.; Nelson, W. H. *J. Phys. Chem. A* **2004**, *108*, 7591

(39) EIE spectra are representative for the partly saturated EPR absorption spectrum with relative line intensities distorted due to in particular cross relaxation effects. The saturation condition leads to an apparent stronger influence of forbidden (or 'second-order') transitions (ref 33) being evident, for example, in Figure 2c.

(40) Close, D. M.; Hole, E. O.; Sagstuen, E.; Nelson, W. H. *J. Phys. Chem. A* **1998**, *102*, 6737.

(41) Box, H. C.; Potter, W. R.; Budzinski, E. E. *J. Chem. Phys.* **1975**, *62*, 3476.

(42) Hüttermann, J.; Ohlmann, J.; Schaefer, A.; Gatzweiler, W. *Int. J. Radiat. Biol.* **1991**, *59*, 1297.

(43) Barnes, J.; Bernhard, W. A.; Mercer, K. R. *Radiat. Res.* **1991**, *126*, 104.

(44) Close, D. M.; Sagstuen, E.; Hole, E. O.; Nelson, W. H. *J. Phys. Chem. B* **1999**, *103*, 3049.

(45) Heller, C.; McConnell, H. M. *J. Chem. Phys.* **1960**, *32*, 1535.

(46) Sagstuen, E.; Hole, E. O.; Haugedal, S. R.; Nelson, W. H. *J. Phys. Chem. A* **1997**, *101*, 9763.

(47) Westhof, E.; Flossmann, W.; Zehner, H.; Müller, A. *J. Chem. Soc., Faraday Trans.* **1977**, *63*, 248.

(48) Malinen, E.; Sagstuen, E. *Radiat. Res.* **2003**, *160*, 186.

(49) Dolgouintcheva, O.; Zakrzewski, V. G.; Ortiz, J. V. *Int. J. Quantum Chem.* **2002**, *90*, 1547.

(50) Lipfert, J.; Llano, J.; Eriksson, L. A. *J. Phys. Chem. B* **2004**, *108*, 8036.

(51) Close, D. M.; Sagstuen, E. *J. Chem. Phys.* **1983**, *79*, 5292.